ELSEVIER

Journal of Nuclear Materials 294 (2001) 299–304

journal of nuclear materials

www.elsevier.nl/locate/jnucmat

Observation of second-phase particles in bulk zirconium alloys using synchrotron radiation ☆

Kenneth T. Erwin [a], Olivier Delaire [a], Arthur T. Motta [a,*], Yong S. Chu [b], Derrick C. Mancini [b], Robert C. Birtcher [c]

[a] *Department of Mechanical and Nuclear Engineering, The Pennsylvania State University, 227 Reber Building, University Park, PA 16802, USA*

[b] *Advanced Photon Source, Argonne National Laboratory, 9700 South Cass Ave, Argonne, IL 60439, USA*

[c] *Materials Science Division, Argonne National Laboratory, 9700 South Cass Ave, Argonne, IL 60439, USA*

Received 3 October 2000; accepted 9 January 2001

Abstract

To further advance the mechanistic understanding of microstructural evolution in zirconium alloys for high burnup applications, it is important to obtain a quantitative measurement of the volume fractions of second-phase precipitates present in the bulk alloys as a function of the heat treatment and irradiation fluence. In this work, X-ray diffraction from a synchrotron radiation source was used to identify and follow the growth kinetics of second-phase particles in zirconium alloys. The high energy flux, energy resolution and signal-to-noise ratio of this light source allowed us to study the very small (<0.2–0.4%) precipitate volume fractions in these alloys. A preliminary calculation of the precipitate volume fraction as a function of cumulative annealing parameter (CAP) showed the precipitate volume fraction increases rapidly above 10^{-19} h and saturates at about 10^{-17} h.

1. Introduction

The types of precipitates present in zirconium alloys used for nuclear fuel cladding, as well as their morphology and distribution, determine the cladding in-reactor behavior, especially corrosion resistance. The structure, size, distribution, and morphology of these precipitates depend on the alloy composition, thermo-mechanical treatment, and irradiation dose. For example, a beta-quench heat treatment leading to small precipitates is known to improve the nodular corrosion resistance of Zircaloy-2 in BWRs and a large precipitate size distribution improves uniform corrosion resistance of Zircaloy-4 in PWRs [1]. However, full mechanistic understanding of the influence of microstructure on the advancement of the corrosion layer in zirconium alloys has not been achieved. One of the problems is that the as-fabricated microstructure present in these alloys has not been fully characterized. In particular, there is not a good estimate of the bulk volume fraction of intermetallic precipitates in the alloys as a function of heat treatment (and, conversely, of the alloying element content in the matrix), and how this volume fraction changes with heat treatment and fluence. Because of the relatively small amount of alloying elements in the matrix, the volume fraction of the second-phase particles is very small (0.2–0.4%). In part because of the difficulty in detecting and quantifying such small volume fractions, there have not been concerted efforts at measuring precipitate volume fractions.

In this work, we show that we can detect these very small amounts of intermetallic precipitates in the bulk material using a synchrotron radiation source. Synchrotron radiation sources provide a much higher flux density than conventional X-ray sources (a factor of 100 or more depending on the beam optics) and energy-tunable capability. The increased flux density allows

☆ Supported by the US Department of Energy, BES, under contract W-31-109-Eng-3B.

* Corresponding author. Tel.: +1-814 865 0036; fax: +1-814 865 8499.

E-mail address: atm2@psu.edu (A.T. Motta).

0022-3115/01/$ - see front matter
PII: S0022-3115(01)00436-6

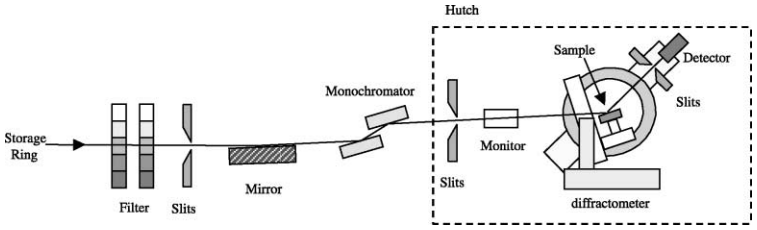

Fig. 1. Experimental setup at the beam line used in this work. The white X-ray beam (an X-ray spectrum of all wavelengths) is generated by synchrotron radiation. The apertured white beam is reflected off a low pass filter with a high-energy cut-off of 20 keV. A double crystal Si (1 1 1) monochromator selects a monochromatic X-ray beam with a bandwidth of about 2 eV. The size of the incident beam is defined by the slits in the hutch and its intensity is measured by the monitor.

data acquisition to be carried out much faster. The higher energy resolution and smaller acquisition times of the synchrotron radiation, compared to conventional X-ray generators, result in a higher signal-to-noise ratio, enabling the detection of very small precipitate volume fractions. This paper presents some of the initial studies aimed at obtaining bulk crystallographic information on the second-phase particles in zirconium alloys, using synchrotron radiation.

2. Experimental methods and sample preparation

The experiments were performed at the Advanced Photon Source synchrotron radiation facility located at Argonne National Laboratory in Argonne, Illinois. The data were collected at the 2-BM bending magnet beamline operated by the Synchrotron Radiation Instrumentation Collaborative Access Team (SRI-CAT). Fig. 1 shows a schematic diagram of this beamline. The incident beam energy of 13 keV (characteristic wavelength = 0.09538 nm) was chosen in order to maximize the penetration of X-rays into the sample without sacrificing the X-ray flux. The incident beam size was 1 mm (vertical) by 3 mm (horizontal). The diffracted beam was measured using a NaI scintillation detector with vertical and horizontal acceptances of 1 and 5 mrad, respectively. The diffraction measurements were carried out using a standard four-circle diffractometer.

Zircaloy-4 sheets were obtained from General Electric, and ZIRLO™ [1] tubing from Westinghouse. Both materials were in the recrystallized state. The samples are polycrystalline (powder-type diffraction), with some degree of texture of the crystallites. The alloy compositions, measured independently by hot vacuum extraction are shown in Table 1. Samples suitable for X-ray diffraction (measuring approximately 10 mm × 5 mm × 0.5 mm) were created by a combination of cutting with a diamond saw and mechanical polishing. The samples were first sealed in quartz, under a high purity Ar atmosphere, and heat-treated in the beta region, at 1273 K for 10 min. The quartz tube was broken so that the samples were quenched in water. The samples were then sealed in quartz under an Ar atmosphere for annealing, to various cumulative annealing parameters (CAPs), defined as

$$\mathrm{CAP} = \sum_i t_i \exp(-Q/RT_i), \tag{1}$$

where t_i(h) is the time at temperature T_i(K), using a Q/R value of 40 000 K [2]. We estimate that the quenched material has a CAP of 7.8×10^{-21} h. Table 2 shows the annealing schedules (time, temperature), and resultant CAP values. All of the samples received a post-anneal mechanical polish using silicon carbide paper with a grit size of 35 μm followed by a final 15 μm grit size polish. The final sample thickness varied from 300 to 700 μm.

Table 1
Measured alloying element content in the zirconium alloys studied in this work (wt.%)

Element	Zircaloy-4 (wt%)	ZIRLO (wt%)
Iron	0.24	0.10
Chromium	0.11	0.001
Tin	1.64	1.08
Nickel	0.0034	<0.001
Oxygen	0.112	0.145
Nitrogen	0.002	0.005
Carbon	0.003	0.002
Silicon	0.0095	0.013
Copper	0.0020	0.0020
Hafnium	<0.004	<0.004
Aluminum	0.0058	0.012
Manganese	<0.001	<0.001
Molybdenum	<0.001	<0.001
Titanium	0.0012	0.0019
Tungsten	<0.004	<0.004
Niobium	–	1.23

[1] ZIRLO is a registered trademark of Westinghouse Electric Company.

Table 2
Annealing schedule and resultant cumulative annealing parameter values for Zircaloy-4

Annealing temperature (K)	Annealing time (h)	CAP (h)
0	0	As-quenched condition (7.8×10^{-21})
818	0.13	7.5×10^{-23}
868	0.11	1.1×10^{-21}
898	0.23	1.0×10^{-20}
963	0.17	1.6×10^{-19}
958	1.70	1.3×10^{-18}
1028	1.00	1.3×10^{-17}
1078	1.60	1.2×10^{-16}

3. Results

Fig. 2 shows the diffracted intensities (arbitrary units) as a function of two-theta angle measured in Zircaloy-4 sheet (CAP $= 10^{-18}$ h), for conventional X-ray (bottom curve) and synchrotron radiation (top curve), after converting the conventional X-ray curve to wavelength as that of synchrotron radiation. The patterns were obtained in θ–2θ geometry with $\phi = 0$ and $\chi = 90$ with the diffraction axis parallel to the sheet normal axis. The X-ray peak locations correspond well with those reported for alpha-Zr and for the hexagonal C14 $Zr(Fe_{1.5}Cr_{0.5})_2$ Laves phase (Joint Committee for Powder Diffraction File #42-1289). These are the stable second-phase intermetallic compound precipitates in Zircaloy-4. The more intense peaks correspond to alpha-Zr; but texturing causes the peak intensities to be modified from the powder diffraction file. Because the diffraction axis is near the sheet normal direction, the basal pole intensities are enhanced with respect to those found in a sample with random orientation. Several precipitate peaks (see the indexing in the picture) are clearly identifiable, in the locations where they do not coincide with the larger Zr peaks.

We note here the difference between the two curves. In the conventional X-ray source, the broadening of the matrix peaks and the lower signal-to-noise ratio cause the precipitate peaks to be much more difficult to distinguish from the background and to quantify. The conventional X-ray scan shown in Fig. 2 was obtained in four hours, while the section of the synchrotron pattern shown in the same figure was obtained in half an hour. It is clear that the synchrotron radiation data is much more precise, and obtained in a time that allows detailed examination of the phenomena.

Fig. 3 shows the diffracted intensities as a function of two-theta angle for a two theta scan of Zircaloy-4 sheet, annealed to a CAP $= 10^{-16}$ h. Note that the bottom scale is linear and the top scale is logarithmic. The relative intensities of the major precipitate peaks observed also differ from the powder diffraction spectra. In particular, the (1 1 2) and (2 0 1) reflections are diminished

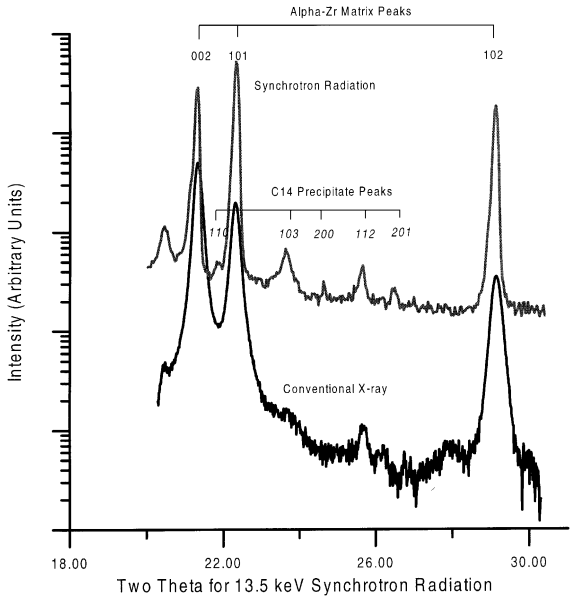

Fig. 2. Diffracted intensity plotted against two-theta angle for Zircaloy-4 annealed to 10^{-18} h, using a conventional X-ray source and using synchrotron radiation.

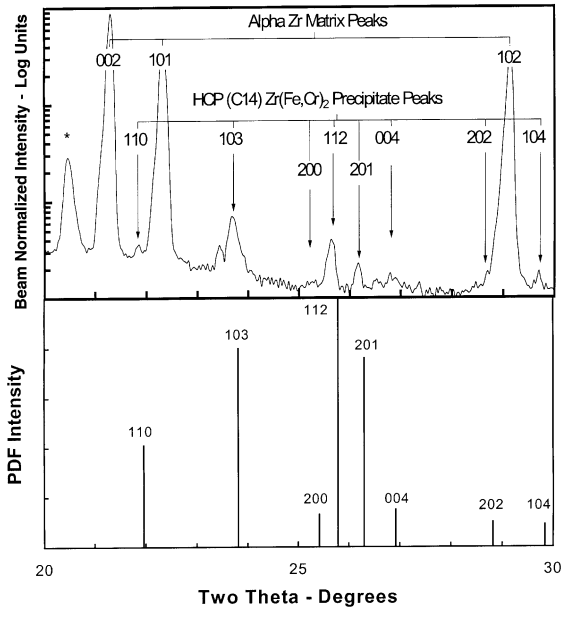

Fig. 3. Two-theta X-ray diffraction pattern for Zircaloy-4 obtained with synchrotron radiation at APS, and reported powder diffraction file intensity for $Zr(Fe_{1.5}Cr0.5)_2$ (Joint Committee for Powder Diffraction File #42-1289) (the asterisk indicates unindexed peaks).

relative to the (1 0 3) reflection. The shift in the relative intensities of the second phases could be due to the texture of the precipitates in the matrix not being completely random or it could also be due to particle counting statistics.

It is noteworthy that these small amounts of precipitates can be detected in the bulk material. Chemical analysis of the alloys studied here (Table 1) shows that the Cr + Fe concentration is 0.35% in Zircaloy-4. Given the relative densities of the alpha-Zr and hcp $Zr(Cr,Fe)_2$ phase (6.5 and 7.5 g/cm^3, respectively), assuming a 3 to 1 Fe to Cr ratio in the precipitates and assuming that all Fe and Cr is precipitated out, we can calculate a theoretical upper bound of the total precipitate volume fraction of 0.46%. If the alloying elements are not completely precipitated, this volume fraction will be lower. These low second-phase volume fractions are very difficult to detect in the bulk and to our knowledge, this is the first reported observations of small precipitate volume fractions by bulk diffraction. We should note that the precipitates diffract more strongly than the matrix so that their peaks are higher than would be expected from a simple proportionality of phase volume fractions, which aided our task.

Fig. 4 shows the X-ray intensities obtained during a two-theta scan of ZIRLO tubing, in a direction close to the radial direction. TEM examinations of ZIRLO performed in the course of this work have identified two main second phases: one a Zr–Nb phase, and another a Zr–Nb–Fe phase, in agreement with previous studies [3]. The Zr–Nb–Fe phase exhibited stacking faults and a similar morphology to the Laves phase $Zr(Cr,Fe)_2$ precipitates in Zircaloy. The peaks for alpha-Zr and beta-Nb phases are clearly identified, as expected, with similar texturing characteristics of the alpha-phase as the Zircaloys. We note that two forbidden peaks of the

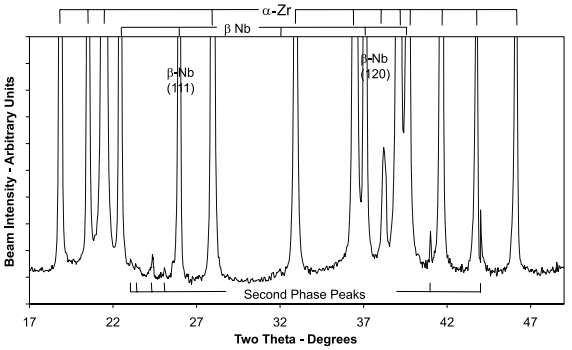

Fig. 4. Two-theta X-ray diffraction pattern for ZIRLO tubing obtained with synchrotron radiation at APS, and expected reflections from second-phase particles with a C14 hexagonal structure and with $a = 0.53$ nm and $c = 0.875$ nm. The energy used for these data was 13.5 keV, so the location of the peaks is slightly shifted from those in the other data in this work.

bcc β-Nb peaks (1 1 1) and (1 2 0) are observed, possibly because of double diffraction. In addition to these, we can observe other peaks, indicated at the bottom of the chart, which we attribute to the intermetallic Zr–Nb–Fe phase. Assuming a hexagonal structure, the peaks attributed to the intermetallic phase can be indexed with lattice parameters $a = 0.53$ nm and $c = 0.875$ nm. Sabol et al. [3] reported an hcp Zr–Nb–Fe phase with $a = 0.54$ nm and $c = 0.87$ nm; consistent with our values. Sabol et al. suggest a stoichiometry of $Zr/(Nb + Fe) \approx 1$ and Nb/Fe1 ≈ 1.33 for this phase. Other researchers have reported a hexagonal $Zr(Nb,Fe)_2$ phase but with a Zr/(Nb+Fe) ratio of 0.5 [4].

Fig. 5 shows the result of X-ray diffraction scans performed on a series of Zircaloy-4 samples that were quenched and annealed to a range of annealing parameters between 7.8×10^{-21} h (quenched state) and 10^{-16} h. The intermetallic precipitates grow upon annealing following quench from the beta-phase, so that higher CAPs result in larger precipitate particles. The spectrum for the 10^{-20} h sample shows matrix peaks, and no discernible precipitate peaks. TEM examinations of this quenched sample show the expected quench microstructure, and no precipitates. The peaks from the alpha phase are very broad, indicating the existence of defects such as grain boundaries, stacking faults and dislocations in the as-quenched alloy, or of micro-strains in the crystal grains. Such defects strain the lattice locally, and the Bragg conditions are relaxed, leading to broader peaks.

As the CAP increases, different peaks start to appear, increase and sharpen. At 10^{-20} h, a broad peak can be seen at approximately 25.5° 2θ. This peak is the (1 1 2) second-phase reflection ($2\theta = 25.785°, I = 100\%$), and is clearly identifiable at CAP $= 10^{-18}$ h. Similarly, the diffraction peak at approximately 23.5° 2θ is clearly identifiable as the (1 0 3) second-phase reflection ($2\theta = 23.817°, I = 80\%$). The integrated intensity of the precipitate peaks increases with increasing CAP, indicating that the total precipitated volume fraction of alloying elements increases with CAP. The peaks become sharper with increasing annealing parameter, indicating that the average precipitate size is increasing.

Fig. 6 shows a preliminary quantification of the precipitation kinetics as measured by the diffraction signal for the Zircaloy-4 sample shown in Fig. 5, performed using the Rietveld method (GSAS program) [5,6]. The Rietveld Method creates a fit to the X-ray data by simultaneously varying several parameters, including crystal structure parameters, scattering factors, and equipment characteristics. We calculated the precipitate volume fraction at each CAP using this method. We give the results in terms of the volume fraction at a given annealing parameter divided by the volume fraction at CAP $= 10^{-16}$ h. The normalized precipitate volume fraction F (precipitate volume fraction at a given value

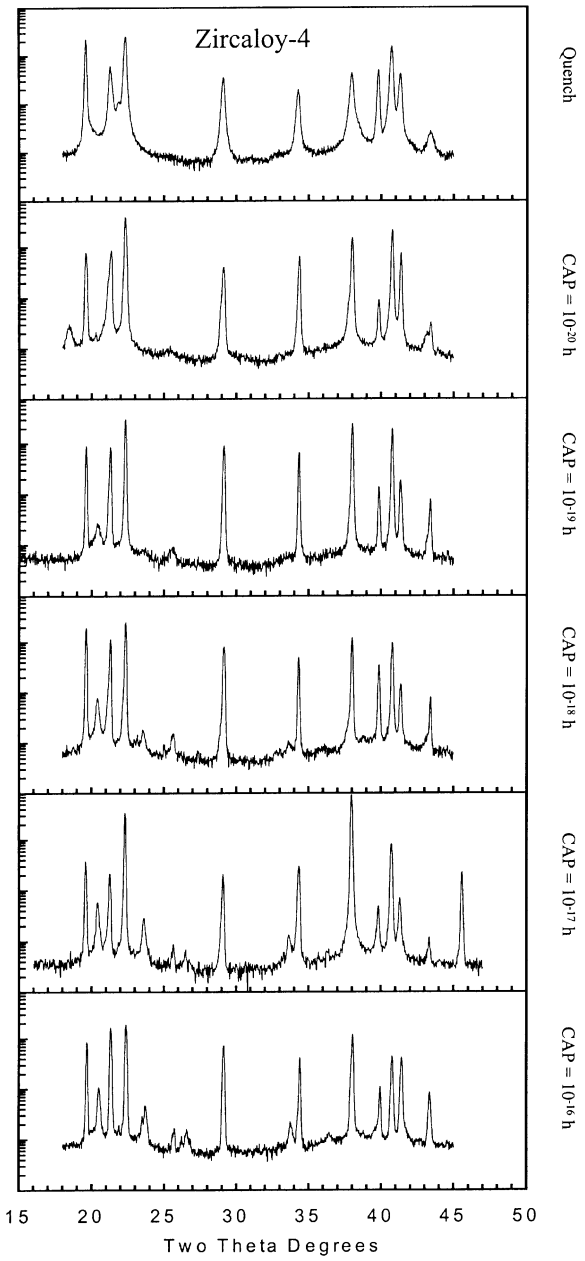

Fig. 5. Two-theta X-ray diffraction scans of Zircaloy-4 obtained on a series of samples with increasing cumulative annealing parameter.

of the CAP, divided by the precipitate volume fraction at 10^{-16} h) is shown plotted against CAP. From the plot it is clear that there is very little precipitation in the as-quenched material and that most precipitation occurs between 10^{-19} and 10^{-17} h. The precipitation kinetics follow an *S*-shape, characteristic of a nucleation and growth precipitation process.

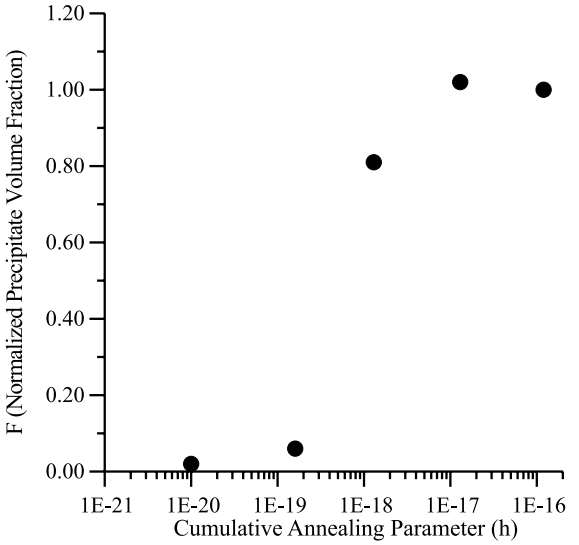

Fig. 6. Precipitate volume fraction in Zircaloy-4 as a function of CAP, calculated from the X-ray spectra shown in Fig. 5, and normalized to the precipitate volume fraction at CAP = 10^{-16} h.

These results show that synchrotron radiation can be used to follow second-phase growth kinetics in zirconium alloys. This observation increases our ability to relate microstructural changes with specific macroscopic effects and opens up several possibilities, including having a true quantitative measure of the precipitate volume fraction as a function of thermo-mechanical treatment, so that processing can be optimized. It also allows the examination of the effect of irradiation on second-phase particle morphology, and stability in bulk samples, thus allowing for a more complete understanding of how irradiation affects cladding behavior by changing its precipitate microchemistry and microstructure.

4. Conclusions

Using the high flux, high resolution, and energy tunable characteristics of the synchrotron X-ray source, we have demonstrated that we can detect small amounts of second-phase particles (0.2–0.4 volume fraction), using bulk X-ray diffraction, even at annealing parameters down in the 10^{-19} to 10^{-20} h range. To our knowledge, this is the first time that these low-levels of precipitates in zirconium alloys were observed using a bulk diffraction technique. Our results have shown agreement with the expected precipitate structures of Zircaloy-4, and with previous studies performed on ZIRLO. Additionally, we were able to follow the precipitate growth kinetics with increasing CAP values. These observations

have the potential of enabling more detailed studies of precipitate growth and aging processes in bulk alloys under thermal annealing and/or irradiation conditions. Future work will include quantifying the amount of second phases from the X-ray diffraction patterns using Rietveld analysis.

Acknowledgements

Thanks are due to R.B. Adamson at G.E. Vallecitos, and G.P. Sabol and R.J. Comstock at Westinghouse Science and Technology Center for furnishing the samples used in this study. A.T.M. would like to acknowledge helpful discussions with R.J. Comstock on synchrotron radiation and with P. Heaney and R. Von Dreele on the use of GSAS. Use of the Advanced Photon Source was supported by the US Department of Energy, Basic Energy Sciences, Office of Science, under Contract No. W-31-109-Eng-38. This research was sponsored by the Department of Energy, Nuclear Engineering Education and Research (DOE-NEER) program, under grant number DE-FG07-98ID 13637.

References

[1] F. Garzarolli, R. Holzer, J. Br. Nucl. Soc. 31 (1992) 65.
[2] J.P. Gros, J.F. Wadier, J. Nucl. Mater. 172 (1990) 85.
[3] G.P. Sabol, G.R. Kilp, M.G. Balfour, E. Roberts, in: Eighth International Symposium on Zirconium in the Nuclear Industry, ASTM STP 1023, San Diego, 1989, p. 227.
[4] V.N. Shishov, A.V. Nikulina, V.A. Markelov, M.M. Peregud, A.V. Kozlov, S.A. Averin, S.A. Koblenkov, A.E. Novoselov, in: Eleventh International Symposium on Zirconium in the Nuclear Industry, ASTM STP 1295, Garmisch-Partenkirchen, Germany, 1996, p. 603.
[5] L.B. McCusker, R.B. Von Dreele, D.E. Cox, D. Louer, P. Scardi, J. Appl. Crystallogr. 32 (1999) 36.
[6] A.C. Larson, R.B. Von Dreele, General structure analysis system (GSAS), Los Alamos National Laboratory, Report LAUR 86-748, 2000.